

See discussions, stats, and author profiles for this publication at: <https://www.researchgate.net/publication/319379312>

# Natural attenuation of Fukushima-derived radiocesium in soils due to its vertical and lateral migration

Article in *Journal of Environmental Radioactivity* · August 2017

DOI: 10.1016/j.jenvrad.2017.06.019

CITATIONS

0

READS

26

12 authors, including:



**Alexei Konoplev**

Fukushima University

142 PUBLICATIONS 1,398 CITATIONS

SEE PROFILE



**Tsugiko Takase**

Fukushima University

23 PUBLICATIONS 106 CITATIONS

SEE PROFILE



**Vasyl Yoschenko**

Institute of Environmental Radioactivity, Fuk...

56 PUBLICATIONS 575 CITATIONS

SEE PROFILE



**Yuichi Onda**

University of Tsukuba

314 PUBLICATIONS 3,626 CITATIONS

SEE PROFILE

Some of the authors of this publication are also working on these related projects:



ANR Amorad [View project](#)

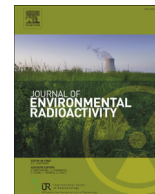


Dynamics of Runoff And Erosion Modelling (DRAEM) [View project](#)



Contents lists available at ScienceDirect

## Journal of Environmental Radioactivity

journal homepage: [www.elsevier.com/locate/jenvrad](http://www.elsevier.com/locate/jenvrad)

## Natural attenuation of Fukushima-derived radiocesium in soils due to its vertical and lateral migration

A. Konoplev<sup>a,\*</sup>, V. Golosov<sup>b</sup>, Y. Wakiyama<sup>a</sup>, T. Takase<sup>a</sup>, V. Yoschenko<sup>a</sup>, T. Yoshihara<sup>c</sup>, O. Parenjuk<sup>d</sup>, A. Cresswell<sup>e</sup>, M. Ivanov<sup>b</sup>, M. Carradine<sup>f</sup>, K. Nanba<sup>a</sup>, Y. Onda<sup>g</sup>

<sup>a</sup> Institute of Environmental Radioactivity, Fukushima University, Kanayagawa 1, Fukushima, 960-1296 Japan

<sup>b</sup> Moscow State University, Faculty of Geography, Moscow, 119991 Russia

<sup>c</sup> Central Research Institute of Electric Power Industry (CRIEPI), Chiba, 270-1194 Japan

<sup>d</sup> Radiobiology and Radioecology Department, National University of Life and Environmental Sciences of Ukraine, Kiev, 08162 Ukraine

<sup>e</sup> Scottish Universities Environmental Research Centre, East Kilbride G75 0QF, UK

<sup>f</sup> Department of Environmental Health and Radiological Sciences, Colorado State University, Fort Collins, CO 80521, USA

<sup>g</sup> Center for Research in Isotopes and Environmental Dynamics, University of Tsukuba, Tsukuba, 305-8572 Japan

## ARTICLE INFO

## Article history:

Received 15 April 2017

Accepted 20 June 2017

Available online xxx

## Keywords:

Radiocesium  
Fukushima  
Watershed  
Floodplain  
Soil  
Sediments  
Migration

## ABSTRACT

Processes of vertical and lateral migration lead to gradual reduction in contamination of catchment soil, particularly its top layer. The reduction can be considered as natural attenuation. This, in turn, results in a gradual decrease of radiocesium activity concentrations in the surface runoff and river water, in both dissolved and particulate forms. The purpose of this research is to study the dynamics of Fukushima-derived radiocesium in undisturbed soils and floodplain deposits exposed to erosion and sedimentation during floods. Combined observations of radiocesium vertical distribution in soil and sediment deposition on artificial lawn-grass mats on the Niida River floodplain allowed us to estimate both annual mean sediment accumulation rates and maximum sedimentation rates corresponding to an extreme flood event during Tropical Storm Etou, 6–11 September 2015. Dose rates were reduced considerably for floodplain sections with high sedimentation because the top soil layer with high radionuclide contamination was eroded and/or buried under cleaner fresh sediments produced mostly due to bank erosion and sediments movements. Rate constants of natural attenuation on the sites of the Takase River and floodplain of Niida River was found to be in range 0.2–0.4 year<sup>-1</sup>. For the site in the lower reach of the Niida River, collimated shield dose readings from soil surfaces slightly increased during the period of observation from February to July 2016. Generally, due to more precipitation, steeper slopes, higher temperatures and increased biological activities in soils, self-purification of radioactive contamination in Fukushima associated with vertical and lateral radionuclide migration is faster than in Chernobyl. In many cases, monitored natural attenuation along with appropriate restrictions seems to be optimal option for water remediation in Fukushima contaminated areas.

© 2017 Published by Elsevier Ltd.

### 1. Introduction

Post-Chernobyl experience has shown that the remediation of radioactively contaminated land should be focused on low cost, low intensity “passive” or low maintenance solutions rather than intrusive, and usually expensive, engineering techniques (IAEA, 2006a; Beresford et al., 2016). Monitored natural attenuation is

an example of such “passive” remediation options relying on natural processes that reduce the flux of radionuclides towards any given receptor (IAEA, 2006b). Processes of natural attenuation do not reduce the total amount of radionuclides in the environment, rather they affect radionuclide distribution over space and time. Physical processes involved in natural attenuation (advection, diffusion, dispersion) may dilute radionuclides in the environment or partially remove/relocate and spread them (wash-off, erosion and sedimentation) (WMO-754, 1992).

On the one hand, contaminated catchments after Fukushima Dai-ichi Nuclear Power Plant (FDNPP) become a long-term source

\* Corresponding author. Institute of Environmental Radioactivity, Fukushima University, Kanayagawa 1, Fukushima, Fukushima Prefecture, 960-1296 Japan.

E-mail address: [r701@ipc.fukushima-u.ac.jp](mailto:r701@ipc.fukushima-u.ac.jp) (A. Konoplev).

of secondary contamination of surface waters (rivers and lakes) due to radionuclide wash-off by surface runoff, both in dissolved and particulate state. Vertical migration of radionuclide in soil leads to contamination of deeper soil layers and penetration of radionuclides to groundwater. On the other hand, processes of vertical and lateral migration lead to gradual reduction in contamination of catchment soil, particularly its top layer (Konoplev et al., 1992; Ivanov et al., 1997; Mishra et al., 2016; Konoplev et al., 2016a). This, in turn, results in a gradual decrease of radionuclide concentrations in the both dissolved and particulate forms of surface runoff and river water (IAEA, 2006c; Bulgakov et al., 2002).

Climate and geographical conditions may essentially influence the rate of natural attenuation processes. In contrast to Chernobyl, Fukushima's watersheds are hilly with steep slopes. Annual precipitation also differs substantially, with annual averages of about 1500 mm/year for Fukushima according to the Japan Meteorological Agency and about 600 mm/year at Chernobyl (Konoplev et al., 2016a).

The fate and transport of accidentally released radiocesium is governed by the ratio of its chemical forms in fallout and site-specific environmental characteristics determining the rates of leaching, fixation-remobilization, as well as sorption-desorption of the mobile fraction (its solid-liquid distribution) (Konoplev et al., 1992; Beresford et al., 2016). Radiocesium in the environment is strongly bound to soil and sediment particles containing micaceous clay minerals (illite, vermiculite etc.). This is due to two basic processes: high selective reversible sorption and fixation (Konoplev and Konopleva, 1999). The proportion of clays is relatively high and reaches up to 30% in Fukushima soils, which is essentially higher than in soils of the Chernobyl zone. There still seems to be no clear understanding of radiocesium speciation in the Fukushima fallout. Adachi et al., 2013 and Abe et al., 2015 have revealed water insoluble spherical glassy aerosol particles greater than 2  $\mu\text{m}$  in diameter, as far as 170 km from the FDNPP, containing, apart from radiocesium, uranium and other elements representative of fuel and reactor materials. Particles of similar properties have also been identified by Niimura et al. (2015) using autoradiography of soils, plants and mushrooms.

After deposition of radionuclides on the ground surface, over time the contamination migrates down through the soil profile. The dynamic pattern of vertical distribution of radionuclides in soil is critical from the standpoint of external dose rate, availability of radionuclides for transfer to surface runoff and wind resuspension in the boundary atmospheric layer, availability of radionuclides for root uptake by plants and percolation to groundwater. Radionuclides migrate vertically in solution and as colloids with infiltration water flow, or attached to fine soil particles (Bulgakov et al., 1991; Konoplev et al., 1992; Bossew and Kirchner, 2004; Mishra et al., 2016). Transport of radiocesium in solution by infiltration is slower than the water flow because of sorption-desorption and fixation on soil particles. Fine soil particles containing radiocesium can move by penetrating through pores, cracks and cavities, as well as with infiltration flow (lessivage), and as a result of vital activity of plants and biota (bioturbation) (Bulgakov et al., 1991; Konoplev et al., 2016b). Nevertheless, the vertical migration of radionuclides in soils unaffected by erosion-accumulation processes can be described by the convection-dispersion equation using the effective values of dispersion coefficient and convective velocity (Konoplev and Golubenkov, 1991; Konshin, 1992).

It is even more challenging to describe radiocesium vertical distribution in soil for the sites with obvious accumulation or loss of soil material as a result of erosion-sedimentation processes, for example, on cultivated slopes or river floodplains. In this case, erosion and/or sedimentation processes have a significant impact on the vertical distribution of radiocesium in soil profile (Walling,

1998; Golosov et al., 2013; Konoplev et al., 2016a; Mamikhin et al., 2016).

Floodplain formation dynamics is primarily influenced by deformation of river channels, sediment transport and load (Schumm, 1985; Lewin, 1978). These, in turn, are governed by hydrological and geomorphological factors, including flood magnitude and frequency, intensity of erosion processes within the drainage area, structure and density of the fluvial net, the grain size composition of the transported sediment, channel morphology and dynamics, width and gradient of the valley floor, and the geological composition of the alluvial valley fill (Blake and Ollier, 1971; Nanson and Croke, 1992; Moody and Troutman, 2000). The main sources of sediments for river basins draining alpine territories with highly forested slopes are mass movement and linear erosion (Wasson and Claussen, 2002; Poesen et al., 2003). Processes of sediment lateral movement on the river bottom include lateral migration, avulsion, meander cutoffs, and channel switching (Nanson and Beach, 1977; O'Connor et al., 2003). The river erodes some sections of floodplain each year, while other sections accrete sediment and gradually rise in elevation above the river bed due to sedimentation (Salo et al., 1986; Hughes, 1997). Quantitative information on floodplain sedimentation rates for short time intervals is limited to several cross-sections or even a single key site (Walling and Bradley, 1989; Ritchie et al., 2004; Mizugaki et al., 2006; Knox, 2006; Golosov, 2009; Golosov et al., 2010).

The purpose of this work is to study dynamics of Fukushima-derived radiocesium in undisturbed soils and floodplain deposits exposed to erosion and sedimentation during floods and estimate the rates of natural attenuation due to radiocesium vertical and lateral migration.

## 2. Material and methods

### 2.1. Study area

The area contaminated after the accident at FDNPP is characterized by a monsoon climate with annual precipitation varying in range from 1100 to 1800 mm/year during 2011–2016 according to the data from five meteorological stations of Japan Meteorological Agency (<http://www.data.jma.go.jp/gmd/risk/obsdl/>) – Haramachi, Iitate, Namie, Tsushima and Tomioka located in contaminated areas. Maximum precipitation occurs during the typhoon season (mid-August - October) and rainy season (late May – mid-July). Temperatures are representative of the monsoon climate with mild winters: the mean monthly values being above zero and with hot, rainy summers. There are actually no periods with soil freezing and, together with large amounts of precipitation in the summer and relatively high average annual air temperature, this should facilitate vertical radiocesium migration in soils (Konoplev et al., 2016a).

Soil diversity in the Fukushima-contaminated areas is great due to the combination of mountain rocks of different lithological composition, intense weathering and denudation from high seismicity, and the steep inclination of mountain slopes. The interfluvial areas include brown soils (under beech forest), ashy-volcanic, rich in humus, acidic allophonic (andosol) and leached brown soils. The valley's bottoms are mainly used as paddy fields and are represented by alluvial soils strongly modified because of many years of land use. Undisturbed alluvial soils occur on the leveed parts of river valley bottoms and along the canalized parts of stream channels typical of intermountain depressions. The arable lands, mainly paddy fields, occupy about 12% of the total territory in the region, and occur primarily on extensive depressions and piedmont lowland.

Fig. 1A shows the study areas and radiocesium deposition based

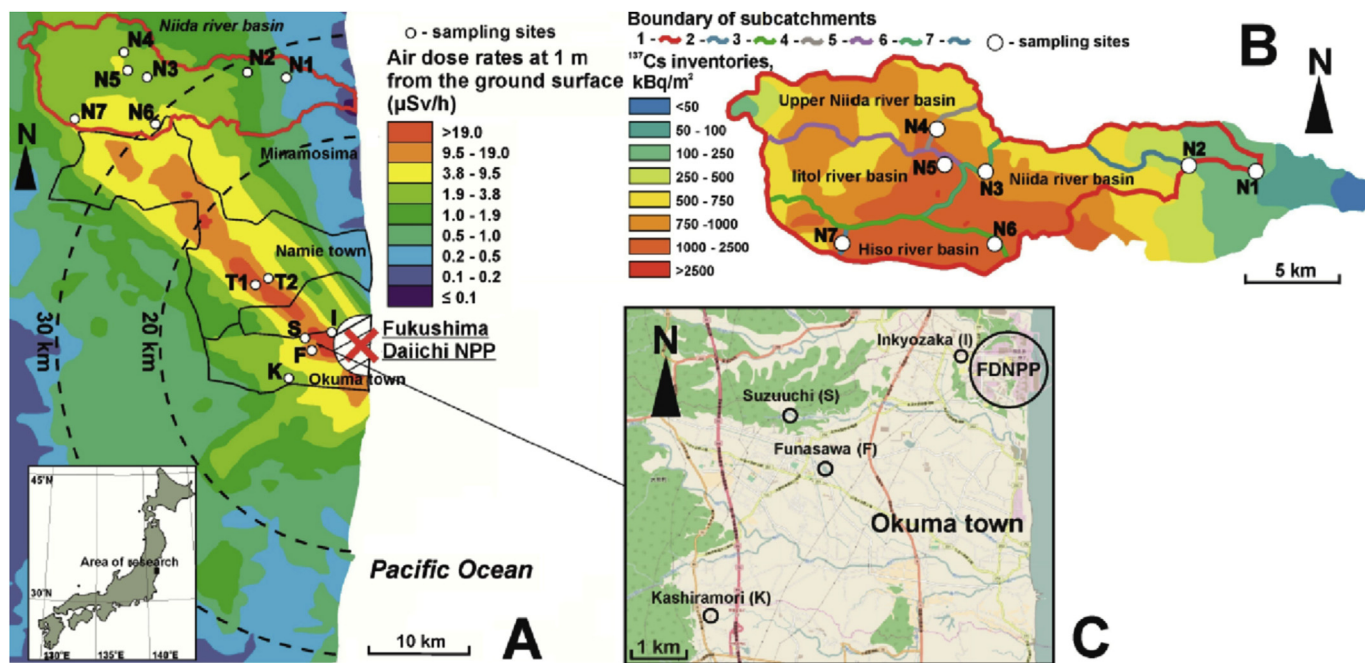


**Fig. 1.** Locations of observation sites with air dose rate distribution map according to the 7th airborne monitoring survey (NRA, 2013) on the date of 28 September 2013 (A); map of Niida river catchment, sub-catchments and sampling sites locations (Golosov et al., 2016; Konoplev et al., 2016b) with <sup>137</sup>Cs deposition levels according to (MEXT, 2011) (B) and location of undisturbed soil sampling sites on the catchments of irrigation ponds Inkyozaka (I), Suzuuchi (S), Funasawa (F) and Kashiramori (K) in Okuma town (Konoplev et al., 2016c).

on the results of the seventh airborne monitoring survey, as of 28 September 2013, (NRA, 2013). Two sampling areas selected for study in the contamination zone were previously described (Konoplev et al., 2016a) - Okuma town and Niida River catchment. One more research area to study dynamics of dose rates was located on the lower parts of a steep slopes of the Takase River catchment in heavily contaminated mixed forest nearby Namie town.

Seven cross-sections for sampling and sediment traps installation were selected on the Niida River floodplain (Fig. 1B). One cross-section characterized the headwaters of the Hiso River basin upstream of its most polluted part (site N7). Three cross-sections integrate the <sup>137</sup>Cs concentration in sediments delivered from headwaters of the main uplands rivers (Upper Niida, Itoi and Hiso, sites N4, N5 and N6 respectively). Two cross-sections are in lower reaches of the Niida River (sites N1 and N2). Site N3 is selected for integration of <sup>137</sup>Cs concentration in sediments transported from both the Itoi and the Upper Niida Rivers at the boundary between headwaters uplands and mid-basin rangelands.

Cores of undisturbed soils have been taken from intact areas of Suzuuchi (S), Funasawa (F) and Inkyozaka (I) pond catchments covered with shrubs and grass. The fourth sampling site was on the forest slope near the pond Kashiramori (K) (Fig. 1C).

The sampling site location was determined with GPS GARMIN Oregon 550TC.

## 2.2. Soil core sampling

Soil cores were collected to a depth of 30 cm using a liner sampler DIK-110C (DAIKI, Japan: [www.daiki.co.jp](http://www.daiki.co.jp)) with a plastic cylinder insert of 5 cm diameter. The soil cores were sliced into layers 1–5 cm thick, depending on layer position, soil density and friability. The upper soil layers were 1–3 cm thick, and the lower layers were 2–5 cm thick. The cores were sampled from April to August 2014, in April 2015 and from June to August 2016 (Table 1).

Soil samples were dried at 50°C for at least 3 days, then ground and homogenized on a mortar.

## 2.3. Application of artificial lawn-grass mats (ALGM)

Square-shaped ALGM (0.46 × 0.46 m<sup>2</sup>) were placed on various levels of floodplain surface within each cross-section if possible in the second half of July 2014 just before the typhoon season. The synthetic grass-lawn had bristles 1.5 cm high to simulate roughness of natural grass cover and to trap sediment. Installation involved natural grass cutting and fixation of ALGM by several steel wire cramps to ensure that the surface was carefully levelled with the surrounding natural grass. Mats were replaced by new ones during the first half of April 2015 after the snowmelt had completed. Therefore, ALGM were exposed to natural sedimentation processes on the Niida River floodplain for two separate periods: first, from July 2014 to April 2015 covering the 2014 typhoon season, and second from April 2015 to July 2015 covering the 2015 rainy season. The thickness of deposited sediment layers on ALGM surface were measured prior to removal. After being removed and delivered to the lab, sediments were rinsed out by tap water and dried, then the total weight of deposits was measured, and the total sediment and radiocesium deposition were calculated. The <sup>137</sup>Cs and <sup>134</sup>Cs concentrations were determined for each sample. This technique was successfully applied to study sediment deposition in different floodplains (Lambert and Walling, 1987; Middelkoop, 1995; Baborowski et al., 2007).

## 2.4. Sample preparation and particle size analysis

Samples of soils and sediments were dried at 60 °C for several days until a constant weight. Then, material was softly crushed using a mortar until complete homogenization of the sample was achieved. Particle size fractions of deposited sediments on ALGM and soils were separated by sieving with sieves of 0.063; 0.1; 0.5;

**Table 1**  
Description of observation and soil sampling sites.

Location	Coordinates	Distance from FDNPP, km <sup>a</sup>	<sup>137</sup> Cs deposition, kBq/m <sup>2</sup>	Soil type**
Inkyozaka (I) pond's catchment	N37.424800° E141.017517°	0.24	2100 ± 1000 (9 soil cores)	Fluvisol
Suzuuchi (S) pond's catchment	N37.415767° E140.979767°	3.75	6400 ± 2200 (8 soil cores)	Fluvisol
Funasawa (F) pond's catchment	N37.406050° E140.986217°	3.5	2900 ± 800 (7 soil cores)	Terrestrial regosol
Kashiramori (K) pond's catchment	N37.379626° E140.959180°	7	900 ± 370 (8 soil cores)	Andosol
Niida river floodplain, N1	N37.654117° E140.956667°	23	110 (MEXT, 2011)	Fluvisol
Niida river floodplain, N2	N37.660908° E140.911855°	27.8	280 (MEXT, 2011)	Fluvisol
Niida river floodplain, N3	N37.653600° E140.798233°	32.2	810 (MEXT, 2011)	Fluvisol
Niida river floodplain, N4	N37.676900° E140.769550°	34.2	960 (MEXT, 2011)	Fluvisol
Niida river floodplain, N5	N37.660700° E140.774583°	32.1	980 (MEXT, 2011)	Fluvisol
Niida river floodplain, N6	N37.613650° E140.801197°	28.6	1660 (MEXT, 2011)	Fluvisol
Niida river floodplain, N7	N37.612845° E140.712493°	34.4	1360 (MEXT, 2011)	Fluvisol
Takase river catchment, T1	N37.465018° E140.920988°	9.8	5800 ± 400 (Backpack)	Andosol
Takase river catchment, T2	N37.471189° E140.935467°	9.0	4400 ± 200 (Backpack)	Terrestrial regosol

<sup>a</sup> Distance was determined from site location to the closest point on the border of FDNPP industrial site; \*\*According to soil classification of Japan (Obara et al., 2011).

1.0 and 2.0 mm mesh. Weight of sediments on each sieve were measured and then weight proportions were obtained. For smaller samples such as individual layers of soil/sediment cores, the laser diffraction particle size analyzer (MASTERSIZER 3000, Malvern Instruments, Ltd., UK) has been used.

### 2.5. Dose rate measurements

Air dose rates at 1 m height were determined at all sites using an ALOKA pocket survey meter PDR-111. A portable gamma spectrometry system in a backpack configuration (Cresswell et al., 2013, 2016; Sanderson et al., 2016) had been deployed to measure dose rates and radiocaesium deposition in forests around the Takase River on 10 April and 18 May 2015. Measurements with this system were repeated at the T1 and T2 sites (Fig. 1A) on 19 October 2015.

D-shuttle dosimeters (Chiyoda Technol Corp., Japan) were used to collect hourly cumulative gamma-ray doses at sites in the Takase river catchment and Niida river floodplain. These dosimeters employ semi-conductor technology using a Si-PIN diode (size of 1.2 cm × 1.4 cm) as the gamma-detector, and are encased in a lead collimated shield (3 cm thick on the top, 3 cm thick of the sidewall and 2 cm thick of the underside) with a 3 cm × 3 cm collimation window in the underside shield opposite the diode. These devices record hourly dose rates inside the collimator, which correlate to the surface dose rate from spots of soil surface (with a diameter approximately equal to the installed height) directly below the collimation window. D-shuttle dosimeters were installed at height of 10 cm–60 cm above the soil surface using specially designed holders. D-shuttle dosimeters were installed at sites T1 and T2 (Takase River catchment) on 19 October 2015 at a height of 10 cm above the floor surface; at site N6 (Niida River floodplain) on 18 February 2016 at a height of 60 cm above the floodplain surface and at site N2 (Niida River floodplain) on 18 February 2016 at a height 20 cm above the floodplain surface. Table 2 presents air dose rates at the sites under study at the time of installation of D-shuttle dosimeters. It should be noted that D-shuttle dose rate readings are essentially lower as compared with air dose rate at 1 m height using ALOKA pocket survey meter PDR-111. However, D-shuttle readings

are much more sensitive to changes in radiocaesium inventory and its vertical distribution on the local spot covered by D-shuttle dosimeter with collimated shield.

### 2.6. <sup>137</sup>Cs and <sup>134</sup>Cs measurements

The <sup>137</sup>Cs and <sup>134</sup>Cs activity concentrations in the samples were measured by gamma spectrometry using a standard electrode co-axial high-purity germanium detector (HPGe) CANBERRA GC3018 with relative efficiency of 31.9%. The gamma-spectra obtained were analyzed with Gamma Explorer (Canberra Industries Inc.). A true coincidence summing correction considering the container geometry was applied. Gamma-ray emissions at energies of 604.7 and 661.6 keV for <sup>134</sup>Cs and <sup>137</sup>Cs, respectively, were counted for 1800–72,000 s (all the samples were measured within 10% error), and detection limits of <sup>134</sup>Cs and <sup>137</sup>Cs were calculated using the method of Cooper. Decay corrections were made based on sampling date. Nine nuclides mixed activity standard volume sources in alumina (Japan Radioisotope Association, Tokyo, Japan; MX0033U8PP) were used as reference standards.

Vertical distributions of <sup>137</sup>Cs in soils were presented as a function of its inventory in 1-cm layer at correspondent depth (Bq/m<sup>2</sup>cm) for floodplain soils or in a fraction of 1-cm layer inventory at correspondent depth from the total <sup>137</sup>Cs inventory in soil (cm<sup>-1</sup>).

## 3. Results and discussion

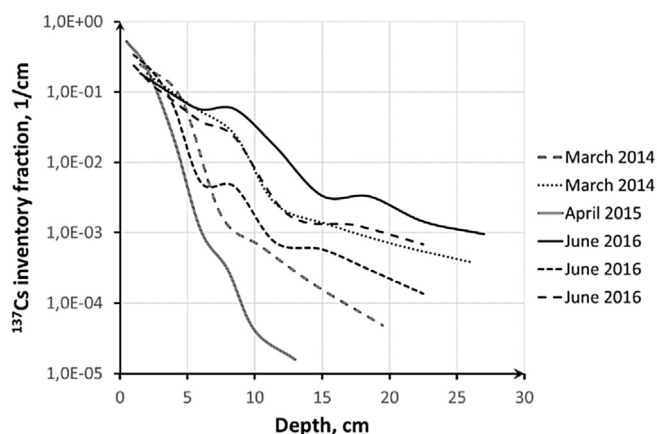
### 3.1. Dynamics of vertical distribution of <sup>137</sup>Cs in undisturbed catchment soils

Fig. 2 presents <sup>137</sup>Cs vertical distributions in six cores of undisturbed grassland soil at the site near the pond Suzuuchi (S) in Okuma town (Fig. 1C), collected from March 2014 to June 2016. All six profiles are characterized by a maximum of <sup>137</sup>Cs activity concentration in the top 2 cm layer of soil, with up to 80–90% of the total inventory remaining in the upper 5 cm layer. The rate of <sup>137</sup>Cs vertical migration in the cores collected shows high variability. The effective dispersion coefficient  $D_{\text{eff}}$  characterizing vertical

**Table 2**

Initial 1-m height air dose rates readings using ALOKA pocket dosimeter for the sites of D-shuttle dosimeters with collimated shield installation for continuous dose rate recording.

Site	Takase river catchment		Niida river floodplain	
	T1	T2	N2	N6
Date of installation	19.10.2015	19.10.2015	18.02.2016	18.02.2016
Air dose rate at 1 m height, $\mu\text{Sv/h}$	18.2	12	0.6	0.85



**Fig. 2.** Differential vertical distributions of  $^{137}\text{Cs}$  inventory fraction ( $\text{cm}^{-1}$ ) in 6 soil cores collected at the site Suzuuchi (S) pond in Okuma town from April 2014 to June 2016.

migration rate in undisturbed soil and estimated using the “quasi-diffusional” model (Bulgakov et al., 1991; Ivanov et al., 1997; Konoplev et al., 2016a) for these six profiles varied in a wide range, from 0.3 to  $3 \text{ cm}^2/\text{year}$ . The lowest  $D_{\text{eff}}$   $0.3 \text{ cm}^2/\text{year}$  was found for the core collected in April 2015, and highest  $3 \text{ cm}^2/\text{year}$  was found for one of the three cores collected in June 2016. Similar variability of  $^{137}\text{Cs}$  vertical distribution and migration rates was observed for other undisturbed soil cores collected in Okuma town (catchments of ponds Inkyozaka, Funasawa and Kashiramori).

It should be said that the profiles shown in Fig. 2 are for the samples collected from March 2014 to June 2016 within one site (at a distance of several meters from each other), which means that the soil type was the same (fluviosol), as well as meteorological conditions (precipitation, air and soil temperature etc.). The observed variability in data, however, is high due to various factors. It needs to be realized that an important role in vertical migration is played by factors which cannot be monitored in a conventional way: these are random processes associated with biota, plant roots etc. Therefore, uncertainty will be high, particularly in the first years after an accident and it does not seem possible to reduce it through monitoring of traditional parameters.

It follows from the above data on  $^{137}\text{Cs}$  vertical distribution in undisturbed catchment soil that both migration parameters and predictions made with them demonstrate a very high uncertainty, at least an order of magnitude, even for the same sampling site. The vertical migration of  $^{137}\text{Cs}$  in Chernobyl soils showed even greater variability (Ivanov et al., 1997). However, as was already noted previously (Konoplev et al., 2016a, 2016b), the range of  $D_{\text{eff}}$  variation in Fukushima-contaminated soils is characterized by higher values.

### 3.2. Study of sediments and associated radiocesium deposition on Niida river floodplain using ALGM

Table 3 summarizes the data obtained using ALGM installed on seven observation sites of the Niida River floodplain. Sedimentation

processes on the floodplain occur exclusively during floods. Both periods of ALGM exposition to sedimentation occurred earlier the extreme flooding caused by Tropical Storm Etau, 6–11 September 2015. According to Japan Meteorological Agency (JMA) during the first period of ALGM installation from July 2014 – April 2015, total of 903 mm of precipitation fell; during the second period of ALGM installation from April 2015 – July 2015, the total precipitation was 370 mm.

A comparison of initial radionuclide inventories in floodplain fluviosols and sediments collected from the ALGM allows us to assess the tendencies of radionuclide inventory change for different reaches of the Niida River basin (Table 2). It is possible to split all sampling locations into three groups according to the proportion of inventory increase: high increase  $>8\%$  (N1/low; N4/middle and N5/middle); medium increase 4–8% (N6/low) and low increase  $<4\%$  (N6/middle and N7/middle). The reasons for such changes, however, even on the floodplain sections forming the same group are different, since sediments accumulation rates and  $^{137}\text{Cs}$  concentrations in deposited sediments were influenced by different factors. There are three main factors influencing radionuclide inventories in sediments: sediment deposition rate, level of radionuclide contamination in the upstream part of the basin and proportion of different sediment sources input. The high increase of total inventories for sampling locations N4 and N5 is mostly associated with the highest deposition rates in these locations (see Table 3). Increased sediment accumulation rates, in turn, are due to the morphology of artificially straightened and narrowed channels on these sites. The watercourse is canalized and the canal has concrete walls. The floodplain is formed within the canal bottom, making the conveying capacity of the channel even lower. As a result, almost every flood event leads to inundation of the floodplain, on which transported sediments tend to accumulate due to high roughness of the surface (grass cover of 0.7–1.0 m high). In fact, these sediments originate from the material transported from the catchment area, which was formed primarily by bank erosion of periodically drying water courses draining the steep slopes on interfluvial area and sediments formed due to partial erosion of sections of floodplain formed on canalized channels. Floodplain sites 4 and 5 (Fig. 1B) are typical of the upper reach of Niida river valley, its main tributary Itoi river and smaller tributaries inflow into these rivers, because these watercourses, except for the uppermost reaches, are running in canalized channels.

Higher levels of radionuclide contamination in the upstream part of the river basin is the main factor for the site N1. N1 located downstream of the Niida river on the lowland plain (Fig. 1B). The lowland plain is the least contaminated part of the Niida basin, and therefore even minor accumulation of relatively low contaminated sediments, of which a large proportion are sediments formed by bank erosion, results in a significant increase in  $^{137}\text{Cs}$  inventory. Sites N6 and N7 are located within the Hiso basin, the central part of which is the most contaminated section on the Niida basin (Fig. 1B). In absolute terms, the  $^{137}\text{Cs}$  concentrations in sediments deposited on these floodplain sections after typhoon seasons and rainfalls are not so much different from those in sediments deposited on sites N4 and N5. The Hiso river, upstream of site 6 and almost all the way to site N7, is running in a partially regulated

**Table 3**  
Total sediment deposition (mm) and changes of  $^{137}\text{Cs}$  inventories for observation sites on the Niida River floodplain using ALGM.

Site	Floodplain level	Layer of deposited sediments, mm	$^{137}\text{Cs}$ deposition with sediments, kBq/m <sup>2</sup>	% of initial inventory
ALGM exposition time from July 2014 to April 2015				
N1	Low	5.2	9.7	8.6
N4	Middle	9.2	91	9.4
N5	Middle	6.8	98	10
N6	Low	2.9	72	4.3
N6	Middle	1.0	43	2.6
N7	Middle	2.0	31	2.5
ALGM exposition time from April 2015 to July 2015				
N2	Low	0.5	6.9	2.5
N4	Middle	3.5	38	4
N5	Middle	2.1	25	2.6
N6	Low	0.5	14	0.8
N7	Low	1.6	30	2.2
N7	Middle	0.3	5.5	0.4

channel and only some parts of one bank are consolidated. The morphology of the floor of the valley is such that the river is eroding the valley sides on many sections and this material resulting from erosion is the main source of the suspended sediment load. In contrast, site N7, located on the Hiso river floodplain upstream of the zone with the highest contamination levels, occurs in a canalized channel, likewise sites N4 and N5. The channel of the Hiso river and its tributaries located upstream of site N7 is draining an extensive intermountain depression and is also canalized. A minor increase in the  $^{137}\text{Cs}$  inventory in this case is explained by low overbank sedimentation rates.

The average annual sedimentation rate of different sections of the Niida River floodplain based on ALGM observations from July 2014 to July 2015 varied from 0 to 1.3 cm/year depending on the site location and floodplain level. This range corresponds to mean values estimated from radiocesium vertical distributions in Niida River floodplain deposits of 2014 (Konoplev et al., 2016a).

Fig. 3 shows the particle size distribution for sediments accumulated and collected on the mats in July 2015 which was measured by sieving. Fig. 4 shows particle size distribution obtained by laser diffraction for the layers of different depths of the core collected at site N5. Since the amount of available material was much more limited, it was not possible to use the sieving method in this case. Comparison of the particle size distributions for the mats and different layers of the core at site N5 indicates that they are more or less identical, having the maximum around 60–100  $\mu\text{m}$ . However, possible errors associated with application of different

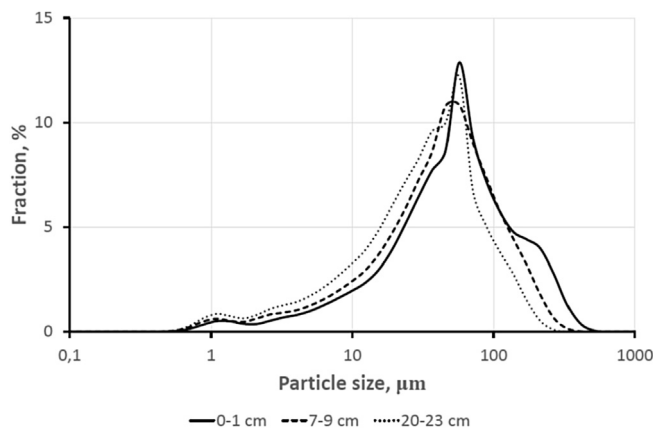


**Fig. 4.** Differential particle size distribution of sediments at various depth (0–1 cm; 7–9 cm and 20–23 cm) measured by laser diffraction particle size analyzer for the core collected near the Niida river waterfront on the site N5.

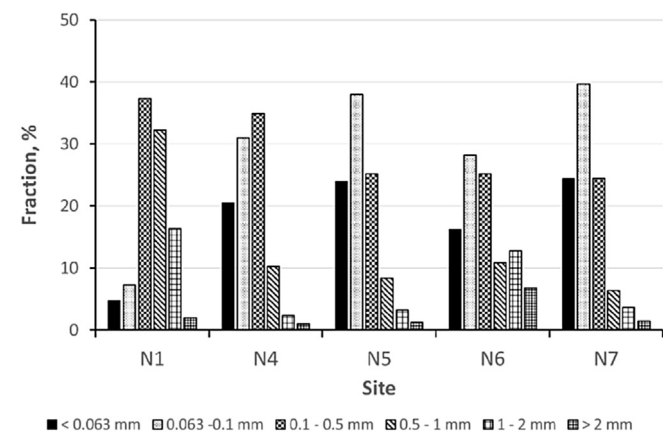


**Fig. 3.** Particle size distribution of sediments deposited and collected on ALGM at Niida river floodplain sites under study. Data were obtained by sieving technique and are presented for the sampling points nearest to the Niida river water front.

techniques for grain size analysis, should be taken into consideration (Konert and Vandenberghe, 1997).

With respect to particle size distribution, the sediments deposited on the mats fall into two groups corresponding to type of channel section on which a site occurs as well as water content of the flow on each of the sections.

Artificial straightened canalized channels form the largest group (sites 4, 5 and 7). Actually, the suspended sediments transported by the flow on these sections are dominated by materials resulting from erosion of the floodplain within the canalized channel with concrete banks. This is confirmed by similar particle sizes of sediments, sampled along the sediment depth profile on the floodplain site 5 (Fig. 4), for which sediment depth profiles were obtained. Very small variations in particle sizes between different layers are explained by certain differences in transporting ability of the flow during floods of different water content. In case of heavier floods, the proportion of sand (0–1 cm layer on Fig. 4) due to somewhat higher fraction of sand in suspended sediments that are redeposited on the floodplain.

Note should also be made of a gradual reduction in fine fractions (<0.1 mm) in sediments from sections with greater water content of river flows from site 7 (upstream of the river Hiso) to site 4 (channel of the river Niida, above the confluence with the river Itoi).

The second group includes sediments on the floodplain (sites 1 and 6) noted for larger particle sizes. These sites are located on the floodplain section downstream of the eroded valley side of the river

Hiso in its lower reaches and on a wide floodplain section in the lower reach of the river Niida on coastal lowland. Particle sizes of these sediments always remain larger as compared to sediments on floodplains of the first group, however, can vary within a wide range depending on strength of floods occurring in a particular section. Flood strength is controlling the ratio of particle sizes of sediments resulting from erosion of valley walls of the river channel, influxes from catchment areas and erosion of floodplain sections. The proportion of sediments formed due to erosion of valley walls and river channel is increasing sharply and becomes dominant during extreme floods, while fine particles of the sediments, due to increased turbulence of flows, do not redeposit on the floodplain at all and are transported downstream.

Particle size distribution on site 1 is also controlled by water content of the river flow which, first, is higher in the lower reaches of the river and therefore the proportion of fractions with particle size, 0.1 mm, by and large, does not redeposit on the floodplain. Secondly, the particle size distribution of the sediments transported by the river Niida flow downstream is always determined by different sources of sediments, likewise particle size distribution on site 6.

### 3.3. Redistribution of radiocesium within Niida River catchment during extreme flood event

As was shown earlier (Konoplev et al., 2016a), the form of radiocesium vertical distribution in floodplain soils differs significantly from that in undisturbed catchment soils because of erosion of top soil and/or accumulation of sediments during floods. Significant flooding occurs in Fukushima Prefecture during typhoon seasons, usually from mid-August - October, and during rainy seasons, in late May-July (Fig. 5). A very rare extreme flood occurred from 6 to 11 September 2015 as a result of Tropical Storm Etau passed on. During a 6 days-period, 456 mm of precipitation fell in upper reach of Niida River (according to JMA data for litate meteorological station) which is about one third of the annual norm. The probability of such extreme floods can be estimated at 4–5% per year (Golosov et al., 2016). During the flood of September 2015, water flows washed out unsupported sections of stream banks. Also, some landslides occurred, mainly on very steep slopes. Sediment originated from the bank erosion, and landslides has very low concentration of  $^{137}\text{Cs}$  because of high proportion of material from deep soil layers. On the straightened sections of rivers, the water levels rose 2–2.2 m above the low water level, thereby watering floodplains to a depth of over 1.2 m. Significant changes occurred on the upper parts of the basin where floodplain sections were confined by a dam on the one side, while the opposite valley side

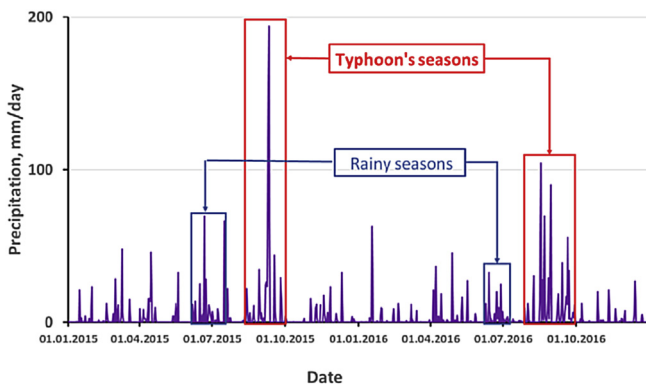


Fig. 5. Precipitation (mm/day) during 2015–2016 at Japan Meteorological Agency's meteorological station litate within Niida river basin (<http://www.data.jma.go.jp/gmd/risk/obsdl/>).

bank was eroded by the river. On separate parts of the river, the flow was discharged within the floodplain and thick sediments were formed of mixed sand and shingle spit of 30–40 cm, with a total weight of 400–500 tons, which is actually one tenth of the total volume of suspended sediments flowing over a year in this cross-section of the Hiso river (right tributary of Niida River) (Fig. 1B, site N6). On the parts of incised riverbed with significant slopes in the middle part of the basin, the water levels were also more than two meters above the low stage, but no major restructuring of the riverbed was seen. The riverbed experienced clearing from meander bars made of sand and gravel material. There were no major changes in the riverbed on the flat part of the basin, even though the maximum water levels on the valley bottom were as high as 2.0–2.5 m above the low water levels. The accumulation layer for sand-gravel and boulder cobble materials on different parts was from 0.1 to 0.5 m, with average values 0.2–0.3 m. (Fig. 1, sites N1 and N2). The length of newly formed sections of meander bars varied from dozens to more than 150 m. On some downstream sections of the Niida River, the banks were eroded over a length of 50–90 m, with dereliction of 2.5 m. It should be noted that the main effect of the flood consisted of strong washing of the Niida River and its tributaries over the entire length of the river up to the estuary, which has led to transport of the most  $^{137}\text{Cs}$  contaminated fine fractions of sediments to the ocean.

Sediment accumulation on different parts of the floodplain has resulted in different changes in dose rates, reflecting the extent to which a specific stretch and adjacent area were contaminated (Table 4). Greater changes in dose rates on the floodplain occurred on the upper reaches.

Fig. 6 demonstrates dynamics of  $^{137}\text{Cs}$  vertical distribution in the upper 30-cm layer of soil/sediments at four selected observation sites on the Niida River floodplain. For the site N2 (Fig. 6A), which is downstream of the Niida River with relatively low radiocesium initial deposition, there was no essential change in  $^{137}\text{Cs}$  inventories during first year of observations from April 2014 to April 2015 (Fig. 4A).  $^{137}\text{Cs}$  inventories in different cores varied in about 10% narrow intervals from 560 kBq/m<sup>2</sup> in April 2014 to 450 kBq/m<sup>2</sup> in April 2015. However, the profile of August 2016 demonstrated significant changes both in the shape of distribution and in  $^{137}\text{Cs}$  inventory.  $^{137}\text{Cs}$  activity concentrations decreased in the top layer from 15 to 20 kBq/kg in 2014–2015 to only 2–3 kBq/kg in 2016 after the extreme flood of September 2015. At the same time, total  $^{137}\text{Cs}$  inventory increased by more than 4 times. 30-cm depth coring was not enough to cover the whole radiocesium profile on site N2 in August 2016, and an essential part of the total  $^{137}\text{Cs}$  inventory was located lower than 30 cm.  $^{137}\text{Cs}$  inventory in upper 30 cm of soil/sediments was found to be 1930 kBq/m<sup>2</sup>. Radiocesium dynamics in soil profile at the site N2 demonstrates, on the one hand, accumulation of contaminated sediments at the site but, on another

Table 4

Change of air dose rate at 1 m height above soil surface at the sites under study within Niida river floodplain before and after extreme flood because of Tropical Storm Etau of September 6–11, 2015

Site	River section	Floodplain section	Air dose rate at 1 m height, $\mu\text{Sv/h}$		
			April 2014	April 2015	April 2016
N1	Downstream	Levee	1.0	0.9–	0.33
		Depression	0.65	0.6	0.6
N2	Downstream	Levee	1.5	1.1	0.6
		Middle level	1.5	1.1	1.0
N3	Upstream	Middle level	2.0	1.3	1.6
N4	Upstream	Middle level	2.5	2.3	0.98
N5	Upstream	Middle level	2.7	2.6	0.85
N6	Upstream	Middle level	5.1	6	0.82
		Higher level	5.1	6	2.1
N7	Upstream	Middle level	3.8	3.7	2.3

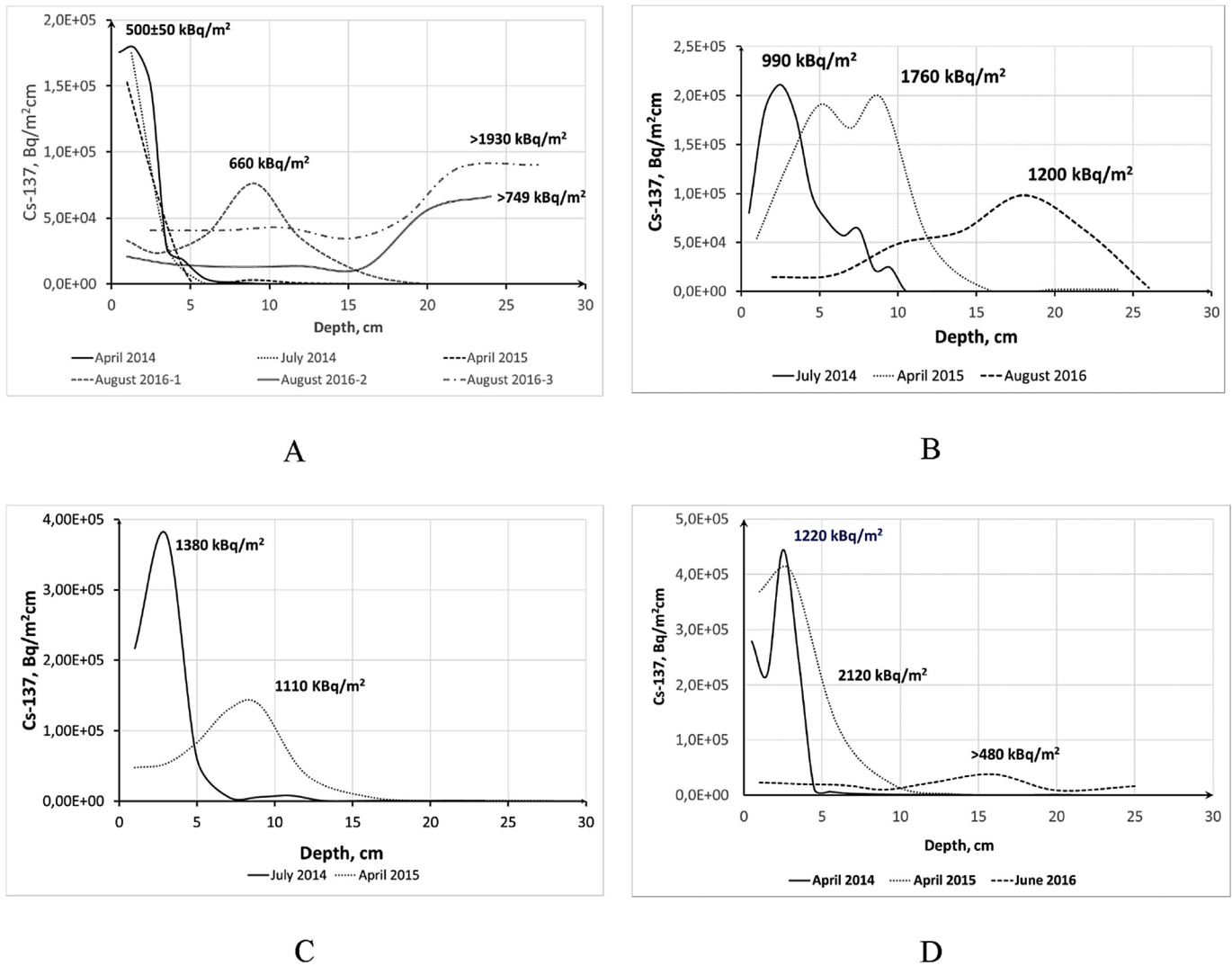


Fig. 6. Dynamics of depth distribution of <sup>137</sup>Cs inventory in 1-cm layer of soil/sediments (Bq/m<sup>2</sup>cm) for Niida river floodplain from April 2014 to August 2016: (A) – site N2 (low level); (B) – site N4 (middle level); (C) – site N5 (middle level); (D) – site N6 (middle level).

hand, substantial reduction of radiocesium activity concentration in top soil layer and covering the most contaminated soil with cleaner “diluted” sediments. Roughly estimated sediment deposition during the flood of September 2015 on the basis of the core collected in August 2016 at the site N2 is about 20 cm.

Vertical distribution of <sup>137</sup>Cs on site N4 (Fig. 6B) has already demonstrated the impact of erosion–sedimentation processes for 2014. From July 2014 to April 2015, the maximum of <sup>137</sup>Cs moved for about 6 cm deeper due to sediments deposition occurring mostly during the 2014 typhoon season. <sup>137</sup>Cs inventory at the site for the same period increased for about 80%, meaning that accumulation processes prevailed erosion. At the same time <sup>137</sup>Cs activity concentration in top soil layer decreased due to deposition of cleaner sediments. As a result of these two opposing processes, increasing of total inventory and decreasing of <sup>137</sup>Cs activity concentration in the top soil layer, the dose rate did not change significantly (Table 4). The core collected in August 2016 showed further movement of the maximum of <sup>137</sup>Cs activity concentration for more 9 cm as compared to the core of April 2015 and substantial decrease of <sup>137</sup>Cs activity concentration in the upper soil layer. The total inventory of <sup>137</sup>Cs dropped to 1200 kBq/m<sup>2</sup> for August 2016 from 1760 kBq/m<sup>2</sup> for April 2015. Most likely, this is explained by a

mixture of processes of upper layer floodplain soils erosion and deposition of fresh, cleaner sediments, mostly occurring during extreme flood event in September 2015. Because of a combination of these processes, the air dose rate at site N4 dropped more than 2 times as compared to 2014 and 2015 (Table 4).

A similar situation was observed for the site N5 (Fig. 6C). A maximum of <sup>137</sup>Cs activity concentration moved deeper for 6 cm from July 2014 to April 2015 and dropped down in absolute value. At the same time, <sup>137</sup>Cs inventory did not change substantially. Unfortunately, it was not possible to collect the core at the site after the extreme flood of September 2015 because this section of floodplain became very stony following the flooding. The reduction of the air dose rate on the site after the extreme flood was about 3 times as compared with 2014–2015 (Table 4).

The most dramatic changes of radiocesium distribution after the extreme flood event in September 2015 occurred at the site N6 on the floodplain of the Hiso River – tributary of Niida River. Fig. 6D demonstrates dynamics of <sup>137</sup>Cs vertical distribution in soil/sediments on the middle level of the floodplain site N6. From April 2014 to April 2015, <sup>137</sup>Cs inventory increased on the site from 1220 kBq/m<sup>2</sup> to 2120 kBq/m<sup>2</sup> because of accumulation of sediments originated from heavily contaminated watershed of upstream Hiso

River. A slight increase of the air dose rate from 5.1 to 6.0  $\mu\text{Sv/h}$  was observed from April 2014 to April 2015, but during the September 2015 extreme flood, these sediments were removed by the flow and were replaced by cleaner sediments originating from deeper soil layers and washout of the unsupported banks. Both activity concentrations and inventory dropped down significantly which caused substantial decrease of the air dose rate from 6 to 0.82  $\mu\text{Sv/h}$  (Table 3). Line measurements of freshly deposited sediments after the flood of September 2015 showed that sediment deposition during the event at site N6 was up to 40 cm.

Therefore, during the extreme flood caused by Tropical Storm Eta occurring during 6–11 September 2015, substantial natural decontamination of the Niida River floodplain took place followed by a significant drop of air dose rate.

### 3.4. Dynamics of $\gamma$ -ray dose rate from soil surface

Fig. 7 shows the dynamics of collimated shield dose rate readings from soil surface on two sites (T1 and T2) on the heavily contaminated Takase River catchment together with data on precipitation and air temperature at meteorological station Namie, located closest to the sites. Dose rate in both cases decreased faster than if due to radioactive decay only. The faster reduction in dose rate is explained by natural attenuation such as erosion of the top soil layer, vertical migration of radionuclides in soil profile and deposition of cleaner sediments transported by surface runoff (IAEA, 2006b). In addition to observed dose rates time dependence, Fig. 5 shows a hypothetical reduction with time of dose rate exclusively due to radioactive decay of  $^{137}\text{Cs}$  ( $T_{1/2} = 30.17$  years) and  $^{134}\text{Cs}$  ( $T_{1/2} = 2.06$  years), which are not subject to any migration, and the change in dose rate is caused by their radioactive decay only. In this case, neglecting the pre-accident radiation background on the sites and assuming that in 2015–2016 observed dose rate can be attributed to  $^{134}\text{Cs}$  and  $^{137}\text{Cs}$  exclusively and the initial ratio of isotopes  $^{134}\text{Cs}/^{137}\text{Cs}$  in fallout immediately after the accident to be 1 (Hirose, 2012), the time change in dose rate can be approximated by the equation below (Yoschenko et al., 2016):

$$DR(t) = DR(t_0) \times \frac{(e^{-\lambda_{137}t} + \alpha_{134} \cdot e^{-\lambda_{134}t})}{(e^{-\lambda_{137}t_0} + \alpha_{134} \cdot e^{-\lambda_{134}t_0})} \quad (1)$$

where  $t$  – current time after the accident;  $t_0$  – time after the

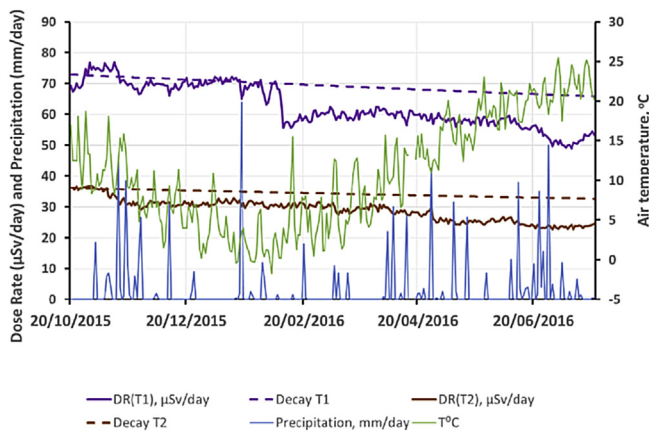


Fig. 7. Time dependence of dose rates ( $\mu\text{Sv/day}$ ) recorded with collimated shield D-shuttle dosimeter from soil surface spot 10 cm below the dosimeter for two sites T1 and T2 on Takase river catchment during eight months from 20/10/2015 to 20/07/2016 together with data on precipitation (mm/day) and air temperature ( $^{\circ}\text{C}$ ).

accident for the date of D-shuttle dosimeter installation;  $DR(t)$  – current dose rate,  $DR(t_0)$  – dose rate for the date of dosimeter installation;  $\lambda_{137}$  and  $\lambda_{134}$  – rate constants of radioactive decay for  $^{137}\text{Cs}$  and  $^{134}\text{Cs}$ , correspondingly;  $\alpha_{134/137}$  – ratio of  $^{134}\text{Cs}$  and  $^{137}\text{Cs}$  gamma kerma equal 2.687 (Gusev and Belyaev, 1991).

Data shown in Fig. 7 are indicative of an essential reduction in dose rate during flooding periods in November 2015 and from the end of May–June 2016. Besides, a significant and sharp reduction in T1 occurred during snowmelt and resulting surface runoff in February 2016, when a sharp increase in air temperature was observed.

Besides processes of radionuclide vertical and lateral migration variations in the daily dose rates over observational period are caused by decay of radionuclides, as well as stochastic nature of quantity measured, changes in  $\gamma$ -ray absorption properties of soil (moisture content), instrument error etc. At the same time, the analysis of time dependence of the ratio of the measured dose rate to the calculated one, based on radioactive decay (equation (1)), shows that for each of the observational sites T1 and T2 three time-intervals can be identified when reduction in dose rate was determined primarily by decay, with minor variations of daily mean dose rates. For the site T1 normalized dose rate was  $1.03 \pm 0.01$  for period from 28 October to 14 November 2015, then it decreased up to  $0.98 \pm 0.03$  for 15 November 2015 to 07 February 2016 and then to  $0.86 \pm 0.02$  for 08 February to 21 June 2016. For T2 the corresponding values were equal to  $1.00 \pm 0.01$  for period 20 October – 08 November 2015;  $0.87 \pm 0.03$  for 09 November 2015–27 April 2016 and  $0.74 \pm 0.03$  for 08 February to 22 July 2016. In all the cases, the differences between the normalized dose rates measured in the subsequent periods were significant ( $t$ -test  $p < 0.00001$ ). Therefore, two sharp reductions in the measured dose rates in each of the observational points were due to a factor other than radioactive decay and cannot be brought about by the above-mentioned factors causing variations of daily mean values. We suppose that these sharp reductions of dose rates in both cases are caused by slope erosion processes associated with heavy rain in November 2015 and snowmelt runoff in February 2016.

For the site N6 on the Niida River floodplain faster reduction of collimated shield dose rate readings as compared to only radiocesium decay was observed as well. However, for the site N2, a slight increase of the D-shuttle dose rate readings was observed due to accumulation of contaminated sediments deposited during flooding.

From the time dependence in D-shuttle dose rate readings an estimated integral rate constant of natural attenuation processes was obtained using an exponential trendline of dose rate dynamics. Calculated rate constants of natural attenuation and its half-times are presented in Table 5. Estimated constants of dose rate reduction for the sites without contaminated sediment accumulation in 2016 ranged from 0.21 to 0.38  $\text{year}^{-1}$  and correspondent periods of dose rate half-reduction was 1.8–3.3 years.

## 4. Conclusions

Application of artificial lawn-grass mats to collect deposited

Table 5

Rate constants  $\lambda_{na}$  ( $\text{year}^{-1}$ ) and half-times  $T_{1/2}^{na}$  (year) of natural attenuation processes based on dynamics of shield collimated dose rate readings.

Site	Period of observations	$\lambda_{na}$ ( $\text{year}^{-1}$ )	$T_{1/2}^{na}$ (year)
Takase river, T1	20.10.2015–20.07.2016	0.32	2.1
Takase river T2	20.10.2015–20.07.2016	0.38	1.8
Hiso river floodplain, N6	20.02.2016–20.07.2016	0.21	3.3
Niida river floodplain, N2	20.02.2016–20.07.2016	–	>5

sediments on the Niida river floodplain allowed sedimentation and radiocesium accumulation rates to be determined at different sections of the floodplain. Integral annual sedimentation rate on different sections of Niida river floodplain based on ALGM observations from July 2014 to July 2015 reached up to 1.3 cm/year depending on the site location and floodplain level. Niida river sections with high, medium and low radiocesium accumulation were identified. During one year from July 2014 to July 2015 up to 13% increase of  $^{137}\text{Cs}$  inventory on the Niida river floodplain was observed using artificial lawn-grass mats.

Extreme flood event of about 4–5% probability associated with Tropical Storm Etou 6–11 September 2015 caused substantial natural decontamination of Niida river floodplain because of erosion of contaminated particles from the top layer and additional burying contaminated surface particles by deposited clean sediments. This was followed by significant drop of air dose rate. Air dose rate at some sections of Niida river floodplain decreased more than 7 times after 6 days of flood. Sediment deposition for downstream section of Niida river floodplain reached 20 cm after the event, and for upstream section in the area of confluence of Hiso river with basic Niida river – up to 40 cm. Extreme flood events during typhoons result in fast and efficient natural attenuation.

Continuous collimated shield dose rate observations from soil surface using D-shuttle dosimeters allowed an estimate natural attenuation rates for river catchments and floodplain radioactive contamination. Estimated rate constants of dose rate reduction for the sites without contaminated sediments accumulation in 2016 were in range of 0.2–0.4 year<sup>-1</sup>.

Accounting for soil erosion and sediment accumulation within river catchment and in particular, river floodplain, is key for predicting redistribution of radioactive contamination after the FDNPP accident on the contaminated territories, as well as for decision making about remediation and clean-up of contaminated territories.

Generally, due to higher precipitation, steeper slopes, higher temperatures and higher biological activities in soils, self-purification and natural attenuation of radioactive contamination in Fukushima associated with vertical and lateral radionuclide migration is essentially faster than in Chernobyl. In many cases monitored natural attenuation along with appropriate restrictions is the most optimal option for water remediation in Fukushima contaminated areas.

## Acknowledgement

The work was funded by the Institute of Environmental Radioactivity at Fukushima University under the project “Radionuclide transport from land to water and its mechanisms” and by Japan Society for Promotion of Science (JSPS), projects 15H0462101 and 15H0403901.

## Appendix A. Supplementary data

Supplementary data related to this article can be found at <http://dx.doi.org/10.1016/j.jenvrad.2017.06.019>.

## References

Abe, Y., Iizawa, Y., Terada, Y., Adachi, K., Igarashi, Y., Nakai, I., 2015. Detection of uranium and chemical state analysis of individual radioactive microparticles emitted from the Fukushima nuclear accident using multiple synchrotron radiation X-ray analyses. *Anal. Chem.* 88, 8521–8525.

Adachi, K., Kajino, M., Zaizen, Y., Igarashi, Y., 2013. Emission of spherical cesium-bearing particles from an early stage of the Fukushima nuclear accident. *Sci. Rep.* 3 <http://dx.doi.org/10.1038/srep02554>.

Baborowski, M., Büttner, O., Morgenstern, P., Krüger, F., Lobe, I., Rupp, H., Tümpling, W.V., 2007. Spatial and temporal variability of sediment deposition

on artificial-lawn traps in a floodplain of the River Elbe. *Environ. Pollut.* 148, 770–778.

Beresford, N., Fesenko, S., Konoplev, A., Skuterud, L., Smith, J.T., Voigt, G., 2016. Thirty years after the Chernobyl accident: what lessons have we learnt? *J. Environ. Radioact.* 157, 77–89.

Blake, D.H., Ollier, C.D., 1971. Alluvial plains of the fly river, Papua. *Z. fuer Geomorphol.* 12 (Suppl. Bd), 1–17.

Bossew, P., Kirchner, G., 2004. Modelling the vertical distribution of radionuclides in soil. Part 1: the convection-dispersion equation revisited. *J. Environ. Radioact.* 73, 127–150.

Bulgakov, A.A., Konoplev, A.V., Popov, V.E., Bobovnikova, Tsl., Siverina, A.A., Shkuratova, I.G., 1991. Mechanisms of the vertical migration of long-lived radionuclides in soils within 30 kilometers of the Chernobyl Nuclear Power Station. *Soviet Soil Sci.* 23 (5), 46–51.

Bulgakov, A.A., Konoplev, A.V., Kanivets, V.V., Voitsekhovich, J.V., 2002. Modelling the long-term dynamics of radionuclides in rivers. *Radioprot. – Colloq.* 37 (C1), 649–654.

Cresswell, A.J., Sanderson, D.C.W., Harrold, M., Kirley, B., Mitchell, C., Weir, A., 2013. Demonstration of lightweight gamma spectrometry systems in urban environments. *J. Environ. Radioact.* 124, 22–28.

Cresswell, A.J., Kato, H., Onda, Y., Nanba, K., 2016. Evaluation of forest decontamination using radiometric measurements. *J. Environ. Radioact.* 164, 133–144.

Golosov, V.N., 2009. Studies of overbank river sedimentation: methodological possibilities and perspectives. *Geomorphologiya* 4, 39–44 (in Russian).

Golosov, V.N., Belyaev, V.R., Markelov, M.V., Kislenco, K.S., 2010. Dynamics of overbank sedimentation rates on floodplains of small rivers of the Central European Russia. In: *Sediment Dynamics for a Changing Future (Proceedings of the ICCE Symposium Held at the Warsaw University of Life Sciences - SGGW, Poland, 14–18 June 2010)*, vol. 337. IAHS Publ., pp. 129–136.

Golosov, V.N., Belyaev, V.R., Markelov, M.V., 2013. Application of Chernobyl-derived  $^{137}\text{Cs}$  fallout for sediment redistribution studies: lessons from European Russia. *Hydrol. Process.* 27, 807–821.

Golosov, V., Botavin, D., Konoplev A., Wakiyama Y., 2016. Geomorphological and radioecological consequences of extreme flood in low-mountainous region of the radioactively contaminated area in subtropical belt (example of Niida River basin, Honshu Island, Japan). *Proceedings of the Conference “Modern Problems of Erosion River Channel and Mouth Processes”, Arkhangelsk (Russia), September 2016*, 35–41 (In Russian).

Gusev, N.G., Belyaev, V.A., 1991. *Radioactive Releases into the Biosphere. Reference book, second ed.* Energoatomizdat, Moscow. 256 p. (in Russian).

Hirose, K., 2012. 2011 Fukushima Dai-ichi nuclear power plant accident: summary of regional radioactive deposition monitoring results. *J. Environ. Radioact.* 111, 13–17.

Hughes, F.M.R., 1997. Floodplain biogeomorphology. *Prog. Phys. Geogr.* 21 (4), 501–529.

IAEA, 2006a. *Environmental Consequences of the Chernobyl Accident and Their Remediation: Twenty Years of Experience. Report of the Chernobyl Forum Expert Group ‘Environment’.* IAEA, Vienna, p. 166.

IAEA, 2006b. *Applicability of Monitored Natural Attenuation at Radioactively Contaminated Sites. Technical Reports Series No. 445.* IAEA, Vienna, p. 105.

IAEA, 2006c. *Radiological Conditions in the Dnieper River Basin. Assessment by an International Expert Team and Recommendations for an Action Plan.* IAEA, Vienna, p. 185.

Ivanov, Y.A., Lewyckyj, N., Levchuk, S.E., Prister, B.S., Firsakova, S.K., Arkhipov, N.P., Arkhipov, A.N., Kruglov, S.V., Alexakhin, R.M., Sandalls, J., Askbrant, S., 1997. Migration of  $^{137}\text{Cs}$  and  $^{90}\text{Sr}$  from Chernobyl fallout in Ukrainian, Belarussian and Russian soils. *J. Environ. Radioact.* 35 (1), 1–21.

Konert, M., Vandenberghe, J., 1997. Comparison of laser grain size analysis with pipette and sieve analysis: a solution for the underestimation of clay fraction. *Sedimentology* 44, 523–535.

Knox, J.C., 2006. Floodplain sedimentation in the upper Mississippi valley: natural versus human-accelerated. *Geomorphology* 79, 286–310.

Konoplev, A.V., Golubenkov, A.V., 1991. Modeling of the vertical radionuclide migration in soil (as a result of a nuclear accident). *Meteorol. i Gidrol.* 10, 62–68 (In Russian).

Konoplev, A.V., Bulgakov, A.A., Popov, V.E., Bobovnikova, Tsl., 1992. Behaviour of long-lived Chernobyl radionuclides in a soil-water system. *Analyst* 117, 1041–1047.

Konoplev, A., Golosov, V., Laptev, G., Nanba, K., Onda, Y., Takase, T., Wakiyama, Y., Yoshimura, K., 2016a. Behavior of accidentally released radiocesium in soil-water environment: looking at Fukushima from a Chernobyl perspective. *J. Environ. Radioact.* 151, 568–578.

Konoplev, A.V., Golosov, V.N., Yoschenko, V.I., Nanba, K., Onda, Y., Takase, T., Wakiyama, Y., 2016b. Vertical distribution of radiocesium in soils of the area affected by the Fukushima Dai-ichi nuclear power plant accident. *Eurasian Soil Sci.* 49 (5), 570–580.

Konoplev, A., Golosov, V., Nanba, K., Omine, K., Onda, Y., Takase, T., Wada, T., Wakiyama, Y., Yoschenko, V., Zheleznyak, M., Kivva, S., 2016c. Radiocesium solid-liquid distribution and migration in contaminated areas after the accident at Fukushima Dai-ichi nuclear plant. In: Ioannidou, A., Povinec, P. (Eds.), *New Challenges with New Analytical Techniques. Proceedings of International Conference on Environmental Radioactivity ENVIRA 2015, Thessaloniki, 21–29 September*, pp. 54–58.

Konoplev, A.V., Konopleva, I.V., 1999. Determination of radiocesium reversible selective sorption characteristics by soils and sediments. *Geochem. Int.* 37 (2),

- 207–214.
- Konshin, O., 1992. Mathematical model of  $^{137}\text{Cs}$  migration in soil: analysis of observations following the Chernobyl accident. *Health Phys.* 63 (3), 301–306.
- Lambert, C.P., Walling, D.E., 1987. Floodplain sedimentation: a preliminary investigation of contemporary deposition within the lower reaches of the River Calm, Devon, UK. *Geogr. Ann.* A69, 393–404.
- Lewin, J., 1978. Floodplain geomorphology. *Prog. Phys. Geogr.* 2, 408–437.
- Mamikhin, S.V., Golosov, V.N., Paramonova, T.A., Shamshurina, E.N., Ivanov, M.M., 2016. Vertical distribution of  $^{137}\text{Cs}$  in alluvial soils of the Lokna River floodplain (Tula oblast) long after the Chernobyl accident and its simulation. *Eurasian Soil Sci.* 49 (12), 1432–1442.
- MEXT (Ministry of Education, Culture, Sports, Science and Technology of Japan), 2011. Results of the Third Airborne Monitoring Survey by MEXT. [http://radioactivity.nsr.go.jp/en/contents/5000/4182/24/1304797\\_0708e.pdf](http://radioactivity.nsr.go.jp/en/contents/5000/4182/24/1304797_0708e.pdf).
- Middelkoop, H., 1995. The impact of climate change on the sedimentation rates on the embanked floodplains in The Netherlands. *Stud. Environ. Sci.* 65, 931–936.
- Mishra, S., Sahoo, S., Bossew, P., Sorimachi, A., Tokonami, S., 2016. Vertical migration of radio- cesium derived from the Fukushima Dai-ichi Nuclear Power Plant accident in undisturbed soils of grassland and forest. *J. Geochem. Explor.* 169, 163–186.
- Mizugaki, S., Nakamura, F., Araya, T., 2006. Using dendrogeomorphology and  $^{137}\text{Cs}$  and  $^{210}\text{Pb}$  radiochronology to estimate recent changes in sedimentation rates in Kushiro Mire, Northern Japan, resulting from land use change and river channelization. *Catena* 68, 25–40.
- Moody, J.A., Troutman, B.M., 2000. Quantitative model of the growth of floodplain by vertical accretion. *Earth Surf. Process. Landforms* 25, 115–133.
- Nanson, G.C., Beach, H.F., 1977. Forest succession and sedimentation on a meandering-river floodplain, northeast British Columbia, Canada. *J. Biogeogr.* 4 (3), 229–251.
- Nanson, G.C., Croke, J.C., 1992. A genetic classification of floodplains. *Geomorphology* 4, 459–486.
- Niimura, N., Kikuchi, K., Tuyen, N.D., Komatsuzaki, M., Motohashi, Y., 2015. Physical properties, structure and shape of radioactive Cs from the Fukushima Daiichi Nuclear Power Plant accident derived from soil, bamboo and shiitake mushroom measurements. *J. Environ. Radioact.* 139, 234–239.
- NRA, 2013. Monitoring Air Dose Rates from a Series of Aircraft Surveys 30 Months after the Fukushima Daiichi NPS Accident. December 25, 2013. Secretariat of Nuclear Regulation Authority. <http://radioactivity.nsr.go.jp/en/contents/9000/8700/view.html>.
- O'Connor, J.E., Jones, M.A., Haluska, T.L., 2003. Floodplain and channel dynamics of the quinnault and queets rivers, Washington, USA. *Geomorphology* 51, 31–59.
- Obara, H., Ohkura, T., Takata, Y., Kohyama, K., Maejima, Y., Hamazaki, T., 2011. Comprehensive soil classification system of Japan first approximation. *Bull. Natl. Inst. Agro-Environ. Sci.* 29, 1–73 (in Japanese with English summary).
- Poesen, J., Nachtergaele, J., Verstraeten, G., Valentin, C., 2003. Gully erosion and environmental change: importance and research needs. *Catena* 50 (2–4), 91–133.
- Ritchie, J.C., Finney, V.L., Oster, K.J., Ritchie, C.A., 2004. Sediment deposition in the flood plain of Stemple Creek Watershed, northern California. *Geomorphology* 61, 347–360.
- Salo, J., Kalliola, R., Hakkinen, I., Neimela, P., Puhakka, M., Coley, P.D., 1986. River dynamics and the diversity of Amazon lowland forest. *Nature* 322, 254–258.
- Sanderson, D.C.W., Cresswell, A.J., Tamura, K., Iwasaka, T., Matsuzaki, K., 2016. Evaluating remediation of radionuclide contaminated forest near Iwaki, Japan, using radiometric methods. *J. Environ. Radioact.* 162–163, 118–128.
- Schumm, S.A., 1985. Patterns of alluvial rivers. *Annu. Rev. Earth Planet. Sci.* 13, 5–27.
- Walling, D.E., Bradley, S.B., 1989. Rates and patterns of contemporary floodplain sedimentation: a case study of the River Culm, Devon, UK. *Geojournal* 19, 53–62.
- Walling, D.E., 1998. Use of  $^{137}\text{Cs}$  and Other Fallout Radionuclides in Soil Erosion Investigations: Progress, Problems and Prospects. Use of  $^{137}\text{Cs}$  in the Study of Soil Erosion and Sedimentation. IAEA-TECDOC-1028. Vienna, 39–62.
- Wasson, R.J., Claussen, M., 2002. Earth system models: a test using the mid-Holocene in the Southern Hemisphere. *Quat. Sci. Rev.* 21 (7), 819–824.
- WMO-754, 1992. Hydrological Aspects of Accidental Pollution of Water Bodies. WMO Operational Hydrology Report No. 37, p. 208.
- Yoschenko, V., Nanba, K., Yoshida, S., Watanabe, Y., Takase, T., Sato, N., Keitoku, K., 2016. Morphological abnormalities in Japanese red pine (*Pinus densiflora*) at the territories contaminated as a result of the accident at Fukushima Dai-ichi Nuclear Power Plant. *J. Environ. Radioact.* 165, 60–67.